European Journal of Medicinal Chemistry 261 (2023) 115837

Contents lists available at ScienceDirect

European Journal of Medicinal Chemistry

journal homepage: www.elsevier.com/locate/ejmech

Research paper

PITB: A high affinity transthyretin aggregation inhibitor with optimal pharmacokinetic properties

Francisca Pinheiro [a], Nathalia Varejão [a,1], Adrià Sánchez-Morales [b,1], Filipa Bezerra [c,d], Susanna Navarro [a], Adrián Velázquez-Campoy [e,f], Félix Busqué [b], Maria Rosário Almeida [c,d], Ramon Alibés [b], David Reverter [a], Irantzu Pallarès [a,**], Salvador Ventura [a,g,*]

[a] Institut de Biotecnologia i Biomedicina and Departament de Bioquímica i Biologia Molecular, Universitat Autònoma de Barcelona, Bellaterra, Barcelona, 08193, Spain
[b] Departament de Química, Universitat Autònoma de Barcelona, Bellaterra, Barcelona, 08193, Spain
[c] Molecular Neurobiology Group, i3S – Instituto de Investigação e Inovação em Saúde, IBMC – Instituto de Biologia Molecular e Celular, Universidade do Porto, 4200-135, Porto, Portugal
[d] Departamento de Biologia Molecular, ICBAS – Instituto de Ciências Biomédicas Abel Salazar, Universidade do Porto, 4050-313, Porto, Portugal
[e] Department of Biochemistry and Molecular & Cellular Biology, and Institute for Biocomputation and Physics of Complex Systems (BIFI), Joint Unit GBsC-CSIC-BIFI, Universidad de Zaragoza, Zaragoza, Spain
[f] Aragon Institute for Health Research, Zaragoza (Spain) and Biomedical Research Network Center in Hepatic and Digestive Diseases (CIBERehd), Madrid, Spain
[g] ICREA, Passeig Lluis Companys 23, E-08010, Barcelona, Spain

ARTICLE INFO

Keywords:
Amyloidosis
Lead optimization
Pharmacokinetics
Stabilizers
Transthyretin
V30M

ABSTRACT

The aggregation of wild-type transthyretin (TTR) and over 130 genetic TTR variants underlies a group of lethal disorders named TTR amyloidosis (ATTR). TTR chemical chaperones are molecules that hold great promise to modify the course of ATTR progression. In previous studies, we combined rational design and molecular dynamics simulations to generate a series of TTR selective kinetic stabilizers displaying exceptionally high affinities. In an effort to endorse the previously developed molecules with optimal pharmacokinetic properties, we conducted structural design optimization, leading to the development of **PITB**. **PITB** binds with high affinity to TTR, effectively inhibiting tetramer dissociation and aggregation of both the wild-type protein and the two most prevalent disease-associated TTR variants. Importantly, **PITB** selectively binds and stabilizes TTR in plasma, outperforming tolcapone, a drug currently undergoing clinical trials for ATTR. Pharmacokinetic studies conducted on mice confirmed that **PITB** exhibits encouraging pharmacokinetic properties, as originally intended. Furthermore, **PITB** demonstrates excellent oral bioavailability and lack of toxicity. These combined attributes position **PITB** as a lead compound for future clinical trials as a disease-modifying therapy for ATTR.

1. Introduction

Amyloid diseases encompass a wide spectrum of disorders characterized by the accumulation of amyloid fibrils, highly organized structures that arise from the misfolding and subsequent aggregation of proteins [1]. Transthyretin amyloidosis (ATTR) is a group of life-threatening systemic disorders caused by the extracellular deposition of transthyretin (TTR) amyloid fibrils [2].

TTR is a 55 kDa homotetrameric protein, which is mainly synthesized in the liver, choroid plexus and retinal pigment epithelium [3,4]. Besides its well-known role as a transporter of thyroxine (T_4) and retinol binding protein-vitamin A complex, TTR is increasingly recognized as having a neuroprotective activity in the central nervous system [5].

The most common forms of ATTR are related with the aggregation of TTR mutants and inherited in an autosomal dominant manner [6]. To date, ATTR onset has been associated with more than 130 genetic variants [7], most of them causing peripheral neuropathy [8] (known as familial amyloid polyneuropathy - FAP) or cardiomyopathy [9] (known as familial amyloid cardiomyopathy - FAC). In some rare cases, TTR mutations can result in leptomeningeal amyloidosis, which is often accompanied by ocular involvement [10].

* Corresponding author. Institut de Biotecnologia i Biomedicina and Departament de Bioquímica i Biologia Molecular, Universitat Autònoma de Barcelona, Bellaterra, Barcelona, 08193, Spain.
** Corresponding author.
E-mail addresses: irantzu.pallares@uab.cat (I. Pallarès), salvador.ventura@uab.cat (S. Ventura).
[1] These authors contributed equally to this work.

https://doi.org/10.1016/j.ejmech.2023.115837
Received 24 July 2023; Received in revised form 24 September 2023; Accepted 26 September 2023
Available online 6 October 2023

Abbreviations

ATTR	transthyretin amyloidosis
FAP	familial amyloid polyneuropathy
FAC	familial amyloid cardiomyopathy
FAP	familial amyloid polyneuropathy
IEF	isoelectric focusing
ITC	isothermal titration calorimetry
TTR	transthyretin

ATTR can also be caused by the wild-type (WT) protein. The deposition of WT-TTR, especially in the heart, underlies the development of senile systemic amyloidosis, a condition that mainly affects elderly man [11]. Senile systemic amyloidosis is gaining recognition as a cause of heart failure, affecting as many as 25% of individuals over 80 years of age [12,13].

Pathogenic mutations in TTR decrease its thermodynamic stability and/or lower the kinetic barrier for tetramer dissociation [14,15], which is considered to be the rate-limiting step in amyloid formation. Occupancy of the T_4-binding sites by specific small molecules is known to stabilize TTR, inhibiting its dissociation and, thus, preventing ATTR onset [16,17]. The so-called kinetic stabilization strategy is the mode of action of the drug tafamidis [18], currently the only pharmacological treatment in the market for both TTR-related polyneuropathy and cardiomyopathy [19,20]. However, the evidence that 30% of patients do not respond to tafamidis [21], together with its high cost [22], has prompted the development of alternative molecules to treat ATTR.

Using a drug repurposing approach, our group identified tolcapone, an FDA-approved drug for Parkinson's disease, as a potent and selective TTR stabilizer, presenting a higher *ex vivo* tetramer stabilizing activity than tafamidis [23]. The results of a Phase IIa clinical trial demonstrated that tolcapone strongly stabilizes TTR in patients with FAP, supporting its further development as a drug to treat ATTR [24,25]. Noteworthy, tolcapone can cross the blood-brain barrier, unlike tafamidis, and it was shown to bind and inhibit the aggregation of the highly destabilized TTR variants associated with leptomeningeal amyloidosis [26].

The higher stabilizing activity of tolcapone compared to tafamidis was attributed to its similar high affinity for both T_4-binding sites, which contrasts with the strong negative cooperativity displayed by tafamidis [27]. Despite tolcapone binds significantly stronger than tafamidis to the second binding cavity, tafamidis affinity for the first cavity is > 3-fold higher. The high-resolution structure of TTR in complex with tolcapone revealed that its 4-methyl-phenyl ring does not establish any enthalpic interaction with the binding pocket, suggesting that there was room for improvement [23]. Building upon this evidence, we have recently synthesized a set of tolcapone-inspired kinetic stabilizers and identified M-23, a molecule that exhibits one of the highest affinities reported for TTR thus far [27]. Yet, a pharmacokinetic (PK) study in mice revealed that M-23 has suboptimal bioavailability (5.5%) and short plasma half-life (0.9 h), which might compromise its therapeutic use.

In the present study, we introduce **PITB** (Pharmacokinetically Improved TTR Binder), a compound designed to address the PK limitations of M-23. PK studies conducted in mice confirmed that, as intended, **PITB** has an excellent PK profile. TTR/**PITB** crystal structures demonstrated the establishment of protein-ligand contacts at the dimer-dimer interface that are absent in tolcapone. These interactions underlie the higher binding selectivity and stabilizing activity showed by **PITB** in serum from both control individuals and TTR V30M carriers, when compared to tolcapone.

Overall, the obtained results underscore the potential of **PITB** as a novel molecule for therapeutic intervention in ATTR.

2. Results and discussion

2.1. Rational design and synthesis of *PITB*

In this study, we aimed at improving the PK properties of M-23 while preserving the primary attributes that enhance its activity relative to tolcapone. Since the new contacts between the lower phenyl ring of M-23 and TTR were proposed to underlie its increased binding affinity and stabilizing activity [27], we kept this ring intact and focused on the 3, 4-dihydroxy-5-nitrophenyl moiety. For tolcapone, the *in vivo* methylation of the 3-hydroxy substituent has been described to generate a long-lived metabolite displaying TTR kinetic stabilizing activity [28,29]. Owing to the chemical similarity between the two compounds, we hypothesized that the methylation of M-23 could also improve its PK profile, while keeping the specific contacts it establishes with TTR (Fig. 1).

In support of this idea and taking advantage of the plasma samples we collected in a previous M-23 PK study in mice, we confirmed that the 3-O-methylation of M-23 occurs *in vivo* and that, remarkably, the resulting derivative exhibited up to 3-fold longer half-life ($t_{1/2}$) in plasma than M-23 (Table 1 and Fig. 2). Of note, M-23 methylation is anticipated to be a minor metabolic route [28], thus being unlikely to contribute to the pharmacological action of M-23. With this in mind, we proceeded to synthesize 3-O-methylM23, which we designated **PITB,** and to analyze its biological activity.

PITB was prepared according to Scheme 1 following an optimized synthetic sequence developed by us [27]. The synthesis leading to **PITB** involves the coupling reaction of the freshly prepared Grignard reagent of iodoarene compound **1** to the methyl diprotected nitro-catechol **2** followed by a Dess-Martin periodinane oxidation reaction to furnish ketone **3** in 58% yield for the two steps. Selective removal of two methyl protecting groups on **3** using BBr_3 in DCM with controlled equivalents of BBr_3 and reaction time delivered the expected monoprotected catechol **PITB** in excellent yield. The structural identity and purity of all compounds were ascertained by NMR spectroscopy and HRMS. The synthesis procedure is detailed in the Experimental Section.

2.2. *PITB* kinetically stabilizes TTR in vitro

We tested whether **PITB** could protect TTR from urea-induced tetramer dissociation. In urea, TTR subunits do not unfold until the tetramer dissociates [30]. At high urea concentrations, tetramer dissociation and monomer unfolding are irreversibly linked, making it possible to evaluate the rate of tetramer dissociation [14,31]. Accordingly, WT-TTR and the two most clinically relevant TTR variants, V30M- and V122I-TTR (1.8 μM) were incubated in the absence or presence of **PITB** (3.6 μM) and TTR denaturation was initiated by adding

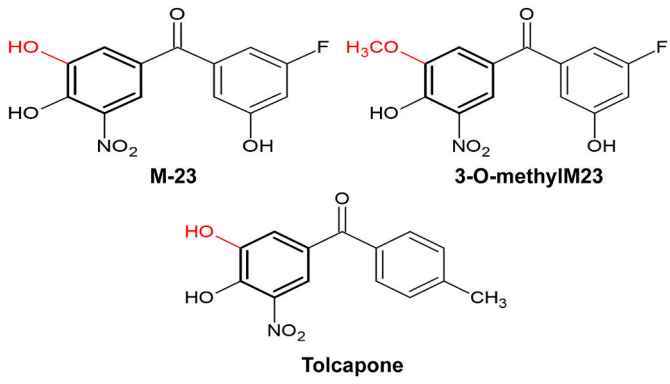

Fig. 1. Chemical structures of M-23, 3-O-methylM23 and tolcapone. The hydroxy group and its methylated form are highlighted in red, and the corresponding phenyl ring is drawn in bold.

Table 1
PK parameters for M-23 and 3-O-methylM23 following intravenous (IV) (1 mg/kg) and oral (PO) (10 mg/kg) administration of M-23 in mice.

	IV (1 mg/kg)		PO (10 mg/kg)	
	M-23	3-O-methylM23	M-23	3-O-methylM23
T_{max} (h)	—	—	< 0.25	< 0.25
C_{max} (ng/mL)	1363.0	555.3	743.7	96.7
AUC_{0-24h} (h·ng/mL)	761.0	462.1	866.4	209.1
$t_{1/2}$ (h)	1.5	2.7	0.9	2.8

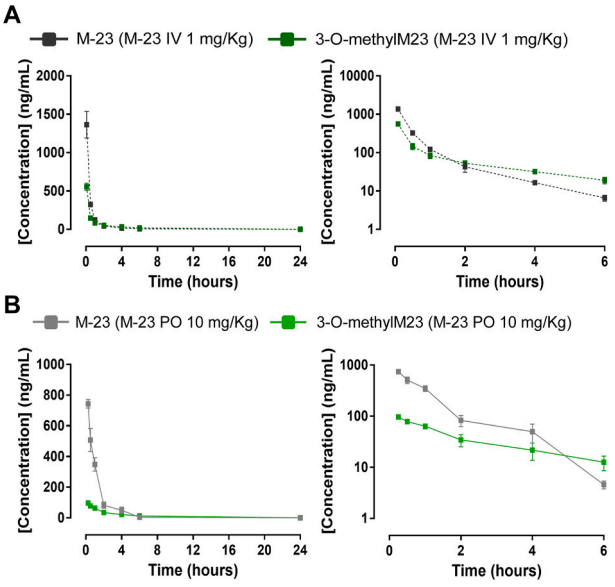

Fig. 2. Plasma concentration-time profiles for M-23 and 3-O-methylM23 after IV (A) and PO (B) administration of M-23 in CD-1 mice. The right panels show the concentration of M-23 and 3-O-methylM23 in plasma up to 6 h after administration of M-23. The y-axis was stretched to a logarithmic scale (without altering the values) to facilitate the comparison between the two compounds. Of note, 3-O-methylM23 was detected after 24 h, in both cases, contrarily to M-23. Data represents mean ± SEM (n = 3).

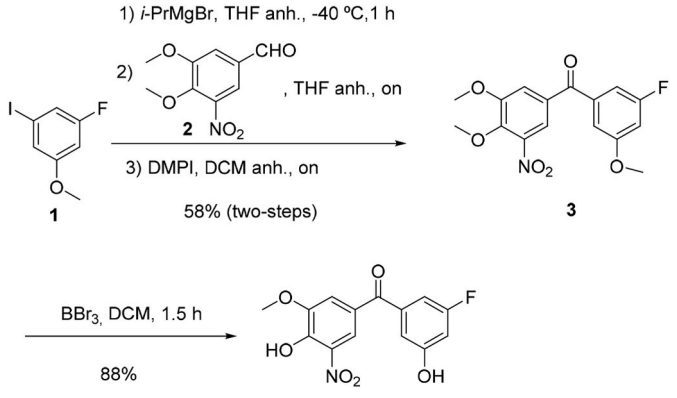

Scheme 1. Synthesis of **PITB**.

urea to a final concentration of 6 M. Tryptophan (Trp) intrinsic fluorescence was measured every 24 h and used to calculate the fraction of unfolded protein (Fig. 3A). The effect of **PITB** was compared with the one of tolcapone.

In the presence of equimolar levels of **PITB** relative to T_4-binding sites, 94.1 ± 0.5%, 79.2 ± 0.2% and 92.5 ± 1.6% of WT-, V30M- and V122I-TTR tetramers, were protected from urea-induced dissociation, respectively. Importantly, **PITB** stabilizing activity was on par with that

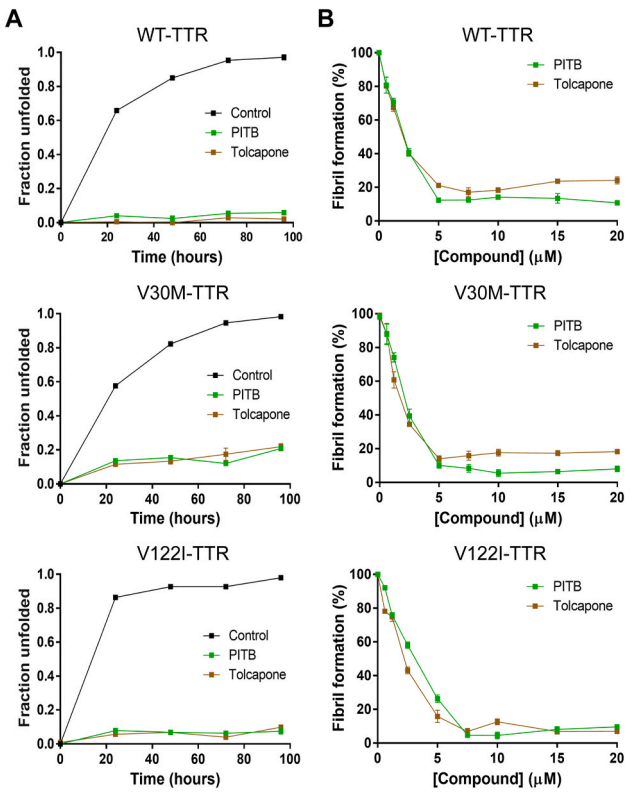

Fig. 3. PITB effect over the kinetic stability and aggregation of WT-, V30M- and V122I-TTR. (A) Unfolding time course at 6 M urea in the absence or presence of 2 molar equivalents of **PITB** and tolcapone, as monitored by Trp fluorescence. The values correspond to mean ± SEM (n = 3). (B) Percentage of TTR aggregation as a function of **PITB** and tolcapone concentration as measured by turbidity at 340 nm. The values were normalized to 100%, which was assigned to the turbidity of samples aggregated in the absence of any compound. Data represents mean ± SEM (n = 3).

exerted by tolcapone for all analyzed TTR variants.

2.3. *PITB protects TTR from aggregation in vitro*

Having established the ability of **PITB** to prevent tetramer dissociation, we proceeded to investigate whether this effect translated into the inhibition of TTR aggregation. For this purpose, TTR samples were mixed with increasing concentrations of **PITB** and aggregation was induced by acidification [31,32]. After an incubation of 72 h at 37 °C, the degree of aggregation was quantified by recording turbidity at 340 nm and normalized to the maximum turbidity value, which was assigned to the TTR samples incubated in the absence of compound (Fig. 3B). The data demonstrate that **PITB** is highly effective at inhibiting the aggregation of WT-TTR and, most importantly, of V30M- and V122I-TTR. In all cases, there was a decrease in TTR aggregation >60% at a 1:1 TTR/**PITB** ratio and ≥87.5% when **PITB** concentration is higher than or equal to the one of T_4-binding sites. Notably, **PITB** outperformed tolcapone, inhibiting up to 89.2% and 92% the aggregation of WT-TTR and V30M-TTR, respectively. In the case of V122I-TTR, **PITB** equaled the potency of tolcapone, reaching up to 90% inhibition at 20 μM.

2.4. *PITB binds with high affinity to TTR*

The high stabilization and anti-aggregation effect of **PITB** on WT-, V30M- and V122I-TTR suggests that it binds with high affinity to these proteins. To determine the binding parameters of **PITB** to TTR, we used isothermal titration calorimetry (ITC). Most ligands bind to TTR with negative cooperativity [18,33,34], which implies that occupancy of the

first binding site results in a reduced affinity for the second site. To account for this possibility, ITC data was analyzed using two models: one considering independent binding to both sites, and the other assuming cooperative binding [35,36].

Our data revealed that **PITB** binds with high affinity and no cooperativity to both WT and TTR variants V30M and V112I (Table 2 and Fig. 4). Moreover, **PITB** binds to WT- and V122I-TTR with an affinity ≥ 3-fold higher than that of tolcapone, and to V30M-TTR with an affinity >12-fold higher. Remarkably, **PITB** presents a significantly higher affinity for V30M- and V122I-TTR than tafamidis [33,37], the only approved kinetic stabilizer for FAP and FAC. Independently of the tested protein, the binding of **PITB** was entirely enthalpically driven ($\Delta H < 0$; $-T\Delta S > 0$), suggesting the establishment of favorable enthalpic non-covalent interactions (e.g., hydrogen bonds or ionic interactions) at the binding interface.

2.5. *PITB stabilizes the weaker TTR dimer-dimer interface*

To elucidate the underlaying interactions that drive the binding of **PITB** to WT-TTR and TTR variants V30M and V122I, we determined the X-ray crystal structures of TTR:**PITB** complexes at 1.85 (WT-TTR:**PITB**), 1.20 (V30M-TTR:**PITB**) and 1.42 (V122I-TTR:**PITB**) Å resolution (Fig. 5). Additionally, we determined the cocrystal structure of tolcapone with V30M-TTR, at a resolution of 1.57 Å. As expected, **PITB** binds to TTR T_4-binding sites at the weaker AB/CD dimer-dimer interface. Because of the two-fold symmetry axis that runs through the binding pockets, two symmetry-related binding conformations appear for **PITB**. In all structures, **PITB** was found in the forward binding mode, with the 3-methoxy-4-hydroxy-5-nitrophenyl pointing to the outer binding cavity, where it makes hydrophobic interactions with the residues from halogen binding pockets (HBPs) 2/2′ and 1/1' (Fig. 5). In this orientation, the 4-hydroxy group of **PITB** forms hydrogen bonds with the K15/K15′ residues of TTR, which in turn stabilize their electrostatic interactions with E54/E54'. These interactions by K15 are also observed in TTR:tolcapone complexes and were proposed to close the binding cavity, protecting the protein-ligand complex from the solvent [23]. In the WT-TTR:**PITB** structure, the hydroxyl side chain of T119 is not at a hydrogen bonding distance from the central carbonyl group, contrarily to what is observed for tolcapone (Fig. 5A). This fact can be explained by the different conformation adopted by the side chain of T119 in the first structure (Fig. S1A). Interestingly, for the same reason, no hydrogen bond is seen between the carbonyl group of both **PITB** and tolcapone, and the side chain of T119, when bound to V30M- and V122I-TTR (Fig. 5B,C and Fig. S1B). On the other hand, **PITB** establishes important interactions in the inner binding cavity, which are not observed in the TTR:tolcapone structures. In particular, the fluorine atom of the 3-fluoro-5-hydroxyphenyl ring interacts with A108, while the hydroxy group forms hydrogen bonds with the S117 residues from adjacent subunits. These additional contacts made by **PITB** likely account for its higher affinity towards WT-, V30M- and V122I-TTR in comparison to tolcapone.

Remarkably, the hydrogen bonds between **PITB** and S117 help to bridge the dimers at the weaker dimer-dimer interface, increasing the kinetic barrier for tetramer dissociation [33,38]. Additionally, in one of the S117 side-chain conformations, a short hydrogen bond can be formed between the S117 residues from adjacent monomers in the same dimer (Fig. S2). This inter-subunit interaction was also observed in the structure of the kinetically stabilized TTR variant T119M [39] and could further contribute to the high stabilizing effect of **PITB**.

2.6. *PITB selectively binds and stabilizes WT-TTR and V30M-TTR in human plasma*

To effectively stabilize the native tetrameric TTR and thus prevent its aggregation in patients with ATTR, **PITB** must selectively bind to TTR in plasma over all other plasmatic proteins. To test this, we examined the capacity of **PITB** to compete with T_4 for TTR binding in human plasma from control individuals (WT-TTR) and individuals carrying the V30M mutation. Tolcapone was included as a control. In this assay, plasma samples were incubated with [^{125}I]-T_4, in the absence or presence of compounds, and subjected to native gel electrophoresis [40]. T_4-binding proteins were detected by autoradiography, as shown in Fig. S3A. In the absence of any compound, three main plasma proteins bound to T_4: the main binding protein was T_4-binding globulin (TBG), followed by albumin (ALB) and TTR. The samples incubated with tolcapone and, especially, **PITB**, presented weaker T_4-TTR bands, indicating that these molecules can compete the binding of T_4 to TTR in human plasma. Densitometry analysis of the bands revealed that **PITB** is a more potent competitor than tolcapone, presenting a displacement of T_4 binding to plasmatic TTR of 97.3 ± 1.2% and 94.5 ± 2.8% for normal plasma or plasma from TTR V30M carriers, respectively (Fig. 6A).

Once we confirmed that **PITB** selectively binds to TTR in human plasma, we investigated its effect on the stability of TTR in the plasma of normal individuals and TTR V30M carriers. The ability of **PITB** to prevent tetramer dissociation was monitored *ex vivo* by isoelectric focusing (IEF) under partially dissociating conditions (4 M urea) [41]. Tolcapone was also used as a control. Briefly, plasma samples were incubated with or without compound overnight at 4 °C and, after IEF, the bands were compared. Under the conditions used, it is possible to distinguish two main sets of bands, one corresponding to monomers (normal and oxidized forms), and one including several bands of lower pI that represent different forms of tetramers (Fig. S3B). The tetramer/monomer ratios were used to calculate the degree of tetramer stabilization in each sample. The results showed that **PITB** has a higher stabilizing activity than tolcapone, especially in plasma from TTR V30M carriers, with an increase in tetramer stability of 17.4 ± 5.1% (versus 4.9 ± 2.3% for tolcapone) (Fig. 6B). The increased binding selectivity and stabilization effect of **PITB** in human plasma, when compared to tolcapone, is likely due to the higher number of interactions it establishes with the protein, as observed in the crystal structure. Additionally, differences in their respective binding to plasma proteins might also contribute to this heightened efficacy.

2.7. *PITB displays no toxicity for human cells*

The assessment of compound toxicity is a crucial aspect in the development of new drugs. Therefore, we conducted experiments to evaluate the potential cytotoxicity of **PITB** using human cervical carcinoma (HeLa) and human hepatoblastoma (HepG2) cells. These cell lines have been extensively studied and used in *in vitro* cytotoxicity studies [42–44]. The HepG2 cell line, in particular, is the most commonly used for detecting drug-induced hepatotoxicity [45,46]. Liver injury is one of the primary causes of drug withdrawal [47] and many medications require monitoring liver function during treatment, including tolcapone

Table 2
Thermodynamic parameters for the interaction of **PITB** with WT-, V30M- and V122I-TTR determined by ITC.

	PITB				Tolcapone			
	Kd (nM)	ΔG (kcal/mol)	ΔH (kcal/mol)	-TΔS (kcal/mol)	Kd (nM)	ΔG (kcal/mol)	ΔH (kcal/mol)	-TΔS (kcal/mol)
WT-TTR	16	−10.6	−13.4	2.8	48	−10.2	−13.6	3.6
V30M-TTR	36	−10.2	−11.0	0.8	440	−8.7	−13.8	5.1
V122I-TTR	14	−10.7	−16.1	5.4	50	−10.0	−12.2	2.2

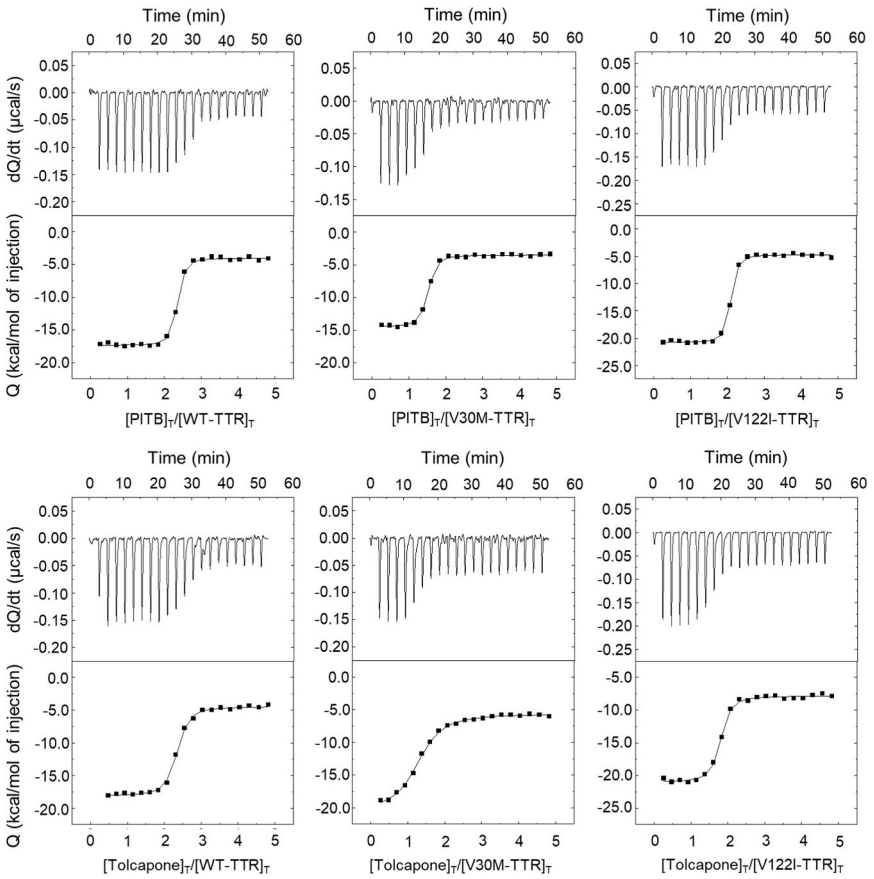

Fig. 4. Interaction of **PITB** with WT-, V30M- and V122I-TTR. The top panels correspond to the raw data after baseline correction, while the lower panels represent the integrated data as a function of the molar ratio between the concentration of **PITB** and protein. The solid lines in the bottom panels represent the best fit to the data to acquire the binding parameters.

[48].

In this study, HeLa and HepG2 cells were incubated with increasing concentrations of **PITB** or tolcapone and cell viability was assessed after 72 h using PrestoBlue®. No significant toxicity was observed in either cell line following exposure to **PITB**, even at the highest concentration of 100 μM (Fig. 7A,B). Importantly, **PITB** was substantially less toxic than tolcapone at concentrations higher than 10 μM, suggesting that **PITB** may be a safer alternative than tolcapone when administered at high doses. To ensure the generalizability of these findings beyond tumor cells, we assessed the cytotoxicity of the two compounds on normal human fibroblast MRC-5 cells (Fig. 7C). The results echoed previous findings, as there was no reduction in the viability of non-tumor cells following **PITB** administration, in stark contrast to the toxic effect of tolcapone.

2.8. PK studies in mice confirm the bioavailability and stability of *PITB*

Altogether, the previous results support the potential of **PITB** to become a drug candidate for the treatment of both hereditary and non-hereditary forms of ATTR. To further explore this option, the PK parameters of **PITB** were determined from studies conducted in CD-1 male mice. The PK profiles for **PITB** following intravenous (IV) (1 mg/kg) or oral (PO) (10 mg/kg) administration of the compound are shown in Fig. 8A, and the calculated parameters are summarized in Table 3. Following the IV injection of **PITB**, a C_{max} value of 4043.3 ng/mL and a $t_{1/2}$ of 3.5 h were determined. Additionally, our results demonstrated that **PITB** is rapidly absorbed after PO administration, reaching a C_{max} of 4176.7 ng/mL, at 0.5 h (T_{max}). While the concentration achieved by the oral route was similar to that observed for the IV infusion, the elimination of **PITB** was considerably slower in this case, with a $t_{1/2}$ of 10.1 h. In both procedures, the concentration of **PITB** in plasma was still quantifiable 24 h post-dosing. The area under the plasma concentration-time curve (AUC) values were 3162.3 h·ng/mL and 26895.9 h•ng/mL for the IV (1 mg/kg) and PO (10 mg/kg) administration of **PITB**, respectively. This indicates an excellent oral bioavailability (%F) of 85.1%, which is significantly higher than the one reported for AG10 (26.8%) in mice following PO administration at 30 mg/kg [33]. Notably, AG10 is a TTR kinetic stabilizer currently undergoing clinical trials for ATTR-related cardiomyopathy.

For comparative purposes, the PK properties of tolcapone after PO administration (10 mg/kg) in CD-1 mice were also determined (Fig. 8B and Table 3). Following administration of equimolar doses of **PITB** and tolcapone, the last was more readily absorbed, achieving a C_{max} of 7616.7 ng/mL in less than 15 min (T_{max}). In contrast, the half-life of **PITB** was significantly higher than the one of tolcapone ($t_{1/2}$ for **PITB** = 10.1 h; $t_{1/2}$ for tolcapone = 1.4 h), which is due to its higher volume of distribution (Vd) and decreased clearance (Cl). Accordingly, no tolcapone was detected in plasma after 24 h. As a result, the exposure to **PITB** was substantially greater than the one to tolcapone ($AUC_{0\text{-}24}$ for **PITB** = 26895.9 h ng/mL; $AUC_{0\text{-}24}$ for tolcapone = 11927.5 h ng/mL).

Overall, these findings indicate that **PITB** exhibits more favorable PK properties than tolcapone, which may potentially translate into improved pharmacological activity *in vivo*.

3. Conclusion

In the present study we have developed **PITB**, a M-23 derivative with optimal PK properties. **PITB** was designed based on the known existence of 3-*O*-methyl tolcapone, a minor metabolite of tolcapone with an increased stability in plasma, and that can act as a TTR stabilizer [28,

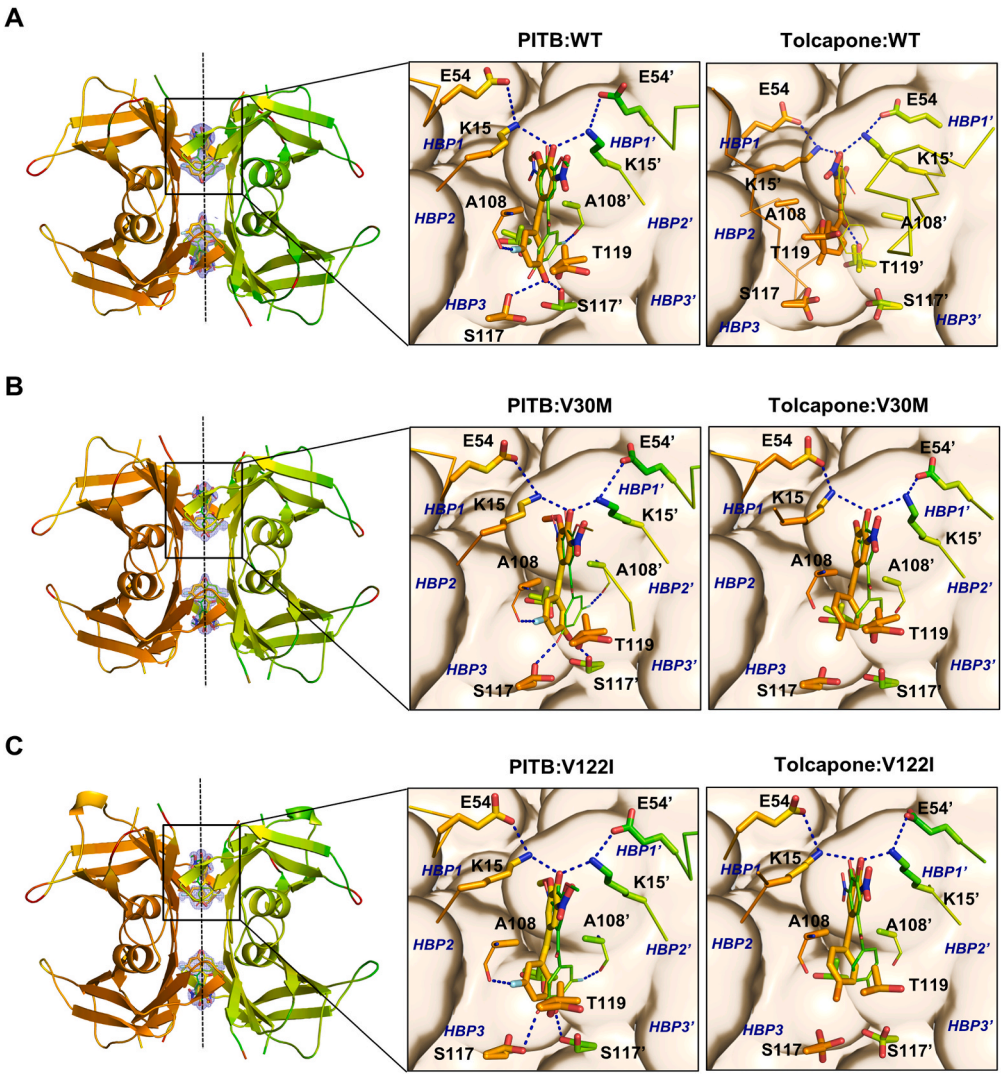

Fig. 5. Crystal structures of WT-TTR (A), V30M-TTR (B) and V122I-TTR (C) in complex with **PITB**. On the left, the global view of TTR bound to **PITB** (cartoon representation). The dashed line corresponds to the twofold symmetry axis of the dimer-dimer interface. The insets show the detailed view of one of the TTR binding sites for **PITB** and for tolcapone. **PITB**, tolcapone and some of the TTR interacting residues are shown as sticks. The dashed blue lines show key interactions between each ligand and TTR. The structural data for Tolcapone:WT and Tolcapone:V122I was obtained from PDB files 4D7B and 5A6I, respectively.

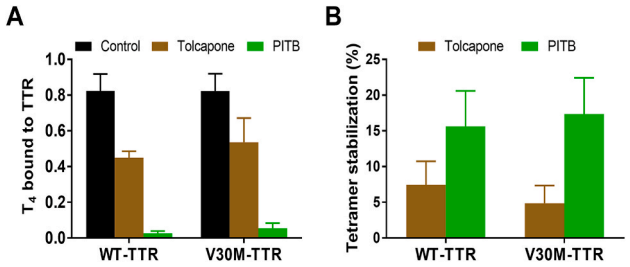

Fig. 6. PITB binding and stabilizing activity in human plasma from control individuals (WT-TTR) or TTR V30M carriers. (A) Fraction of [^{125}I]-T_4 bound to TTR determined by densitometry analysis of the native gel electrophoresis, as explained in the experimental section. The values were normalized to the negative control and correspond to mean ± SEM (n = 3). (B) Percentage of TTR tetramer stabilization calculated from the densitometry analysis of the IEF gels, as detailed in the experimental section. Error bars represent SEM of mean values (n = 2 for WT plasma; n = 3 for V30M plasma).

29]. Since methylation is a common pathway in the metabolism of catechol-containing compounds [49], we hypothesized and confirmed that M-23 has a similar fate. Here, we show that **PITB** binds strongly to the T_4-binding sites of WT-TTR and the two most clinically relevant TTR variants V30M and V122I. As a result, **PITB** greatly increases the stability of TTR tetramers, inhibiting their aggregation. Remarkably, compared with tolcapone, **PITB** presents a higher binding selectivity and stabilization potency in plasma. The high-resolution crystal structures of TTR:**PITB** complexes confirmed that, as intended, **PITB** keeps the critical interactions established by M-23, contributing to its improved efficacy in plasma relative to tolcapone. Additionally, our cytotoxicity assays suggest a low risk associated with **PITB** administration. Most importantly, the PK evaluation of **PITB** in mice revealed a favorable PK profile, with a half-life of 10.1 h and an oral bioavailability of 85.1%. Remarkably, **PITB** demonstrates superior PK parameters when compared to tolcapone, an FDA-approved drug, encouraging future *in vivo* studies, including sex-specific toxicity and efficacy evaluations. Interestingly, **PITB** is prone to undergo 3-O-demethylation *in vivo* [50], originating M-23, which would further sustain its kinetic stabilizing activity.

All in all, the findings presented here underscore the strong potential of **PITB** as a therapeutic agent for ATTR, particularly in cases of FAP

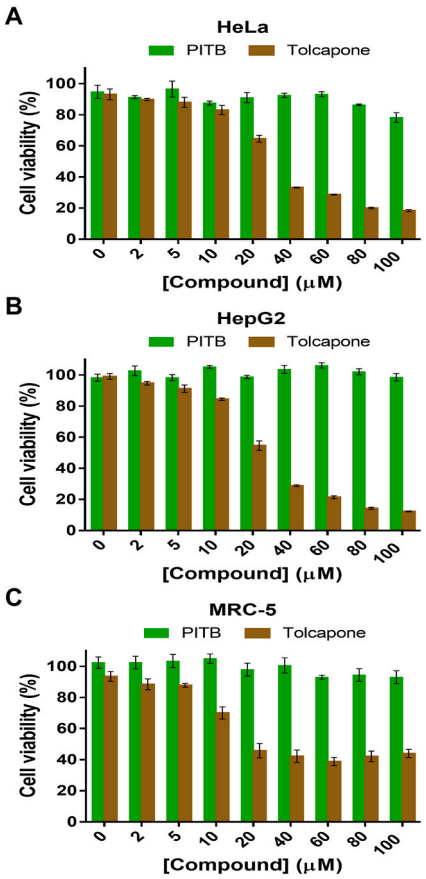

Fig. 7. Toxicity of **PITB** to different cell lines. Cell viability of HeLa (A), HepG2 (B) and MRC-5 (C) cells after 72 h exposure to **PITB** or tolcapone as assessed by the PrestoBlue assay. Data represents mean ± SEM (n = 3).

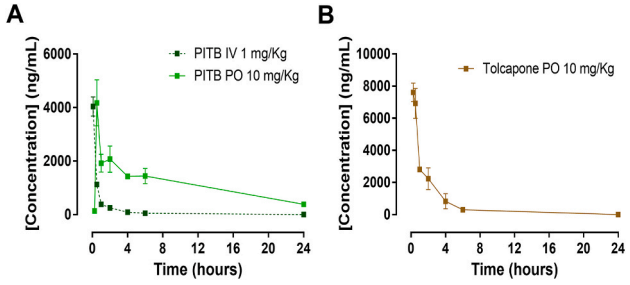

Fig. 8. Plasma concentration-time profiles for **PITB** and tolcapone after administration in CD-1 mice. (A) PK profiles for **PITB** following IV (1 mg/kg) and PO (10 mg/kg) administration. Data represents mean ± SEM (n = 3). (B) Mean plasmatic levels of tolcapone (±SEM) over 24 h after PO administration (10 mg/kg) (n = 3). Noteworthy, no tolcapone was detected after 24 h.

Table 3
PK parameters of **PITB** and tolcapone following administration in CD-1 mice.

	PITB		Tolcapone
	IV (1 mg/kg)	PO (10 mg/kg)	PO (10 mg/kg)
T_{max} (h)	–	0.5	< 0.25
C_{max} (ng/mL)	4043.3	4176.7	7616.7
AUC_{0-24h} (h·ng/mL)	3162.3	26895.9	11927.5
$t_{1/2}$ (h)	3.5	10.1	1.4
k_e (h^{-1})	0.201	0.069	0.500
Vd (L/kg)	1.572	4.482	1.600
Cl (L/h·kg)	0.315	0.308	0.800
F (%)	–	85.1	–

caused by V30M-TTR - the most prevalent mutation in hereditary ATTR cases. Considering that tolcapone has already demonstrated efficacy in a phase IIa clinical trial in this genetic background and given that **PITB** outperforms this drug in nearly every analyzed aspect, our results provide compelling support for further preclinical and clinical development of **PITB**.

4. Experimental section

4.1. General methods

Commercially available reagents were used as received. Solvents were dried by distillation over the appropriate drying agents. All reactions were monitored by analytical thin-layer chromatography (TLC) using silica gel 60 precoated aluminum plates (0.20 mm thickness). Flash column chromatography was performed using silica gel Geduran® SI 60 (40–63 μm). ^{1}H NMR, ^{19}F NMR and ^{13}C NMR spectra were recorded at 250, 400 MHz and 90, 100 MHz, respectively. ^{1}H NMR spectra were referenced to the residual proton signals of CDCl3, 7.26 ppm, and acetone-d_6 2.05 ppm. ^{13}C NMR spectra were referenced to the residual ^{13}C signal of $CDCl_3$, 77.16 ppm, and acetone-d_6, 29.84 ppm. The purity of the **PITB** was determined to be over 95% by HPLC analysis (see the Supplementary Data). Melting points were determined on hot stage and are uncorrected. HRMS were recorded using electrospray ionization (ESI).

4.2. Synthesis procedure

Tolcapone was purchased from Fisher. **PITB** was prepared as described below.

4.2.1. (3,4-Dimethoxy-5-nitrophenyl) (3-fluoro-5 methoxyphenyl) methanone (3)

To a solution of **1** (2.50 g, 9.93 mmol) in dry THF (25 mL) at −40 °C, iPrMgBr (1 M in THF, 15.9 mL, 11.92 mmol) was added dropwise under an Ar atmosphere and the reaction mixture was stirred for 1 h. Then, a solution of 3,4-dimethoxy-5-nitrobenzaldehyde, 2, (2.53 g, 12.00 mmol) in dry THF (20 mL) was added and the mixture was warmed to rt and stirred overnight. The reaction was quenched by the slow addition of brine (20 mL) and the aqueous layer was extracted with EtOAc (3 × 35 mL). The resulting organic layer was dried over anhydrous Na_2SO_4 and concentrated under vacuum to furnish the corresponding alcohol as a yellow oil (1.98 g) which was used in the next step without further purification. To a solution of the alcohol (1.98 g, 5.87 mmol) in dry CH_2Cl_2 (90 mL) under an Ar atmosphere, a solution of DMPI (5.08 g, 12.03 mmol) in dry CH_2Cl_2 (30 mL) was added dropwise and the mixture was stirred overnight at rt. The reaction was quenched with the addition of 12 mL of a prepared solution of $Na_2S_2O_3$ (17.0 g) in a saturated aqueous solution of $NaHCO_3$ (80 mL) and the mixture was stirred for 15 min. The aqueous phase was extracted with CH_2Cl_2 (3 × 50 mL) and the combined organic extracts were dried over anhydrous Na_2SO_4 and concentrated under vacuum. Purification by flash column chromatography (hexanes/EtOAc, 5:2) of the resulting residue provided the ketone **3** as a white solid (1.92 g, 5.72 mmol, 58% yield for the two-steps). **3**: Mp 96–94 °C (from $CHCl_3$). ^{1}H NMR (400 MHz, $CDCl_3$) δ 7.67 (d, J = 2.0 Hz, 1H), 7.62 (d, J = 2.0 Hz, 1H), 7.06 (m, 1H), 7.02 (ddd, J = 8.4 Hz, J = 2.3 Hz, J = 1.4 Hz, 1H), 6.86 (dt, J = 10.2 Hz, J = 2.3 Hz, 1H), 4.06 (s, 3H), 3.97 (s, 3H), 3.84 (s, 3H); ^{19}F NMR (250 MHz, $CDCl_3$) δ −110.1 (s); ^{13}C NMR (90.5 MHz, $CDCl_3$) δ 192.4 (d, J = 2.8 Hz), 163.3 (d, J = 248.3 Hz), 161.1 (d, J = 10.8 Hz), 154.4, 146.7, 144.2, 139.0 (d, J = 8.4 Hz), 132.0, 118.7, 116.3, 111.2 (d, J = 2.8 Hz), 109.1 (d, J = 23.1 Hz), 106.4 (d, = 25.0 Hz), 62.4, 56.8, 56.1. HRMS (ESI+) calcd. for $[C_{16}H_{14}FNO_6+Na]^+$ 358.0703; found $[M+Na]^+$ 358.0705.

4.2.2. (3-fluoro-5-hydroxyphenyl) (4-hydroxy-3-methoxy-5-nitrophenyl) methanone, ***PITB***

BBr_3 (1 M in CH_2Cl_2, 9.50 mL, 9.50 mmol) was added dropwise to a solution of **3** (400 mg, 1.19 mmol) in CH_2Cl_2 (6.0 mL) at −10 °C. The reaction was allowed to proceed at rt for 1.5 h (TLC, CH_2Cl_2/MeOH, 10:1). The reaction was quenched with water (8 mL) and the resulting aqueous layer was extracted with EtOAc (2 × 20 mL). The organic extracts were dried with anhydrous Na_2SO_4 and the solvent removed under vacuum to give the crude product which was purified by flash column chromatography (CH_2Cl_2/MeOH, 20:1) to afford **PITB** as a yellow solid (311 mg, 1.01 mmol, 85% yield). Mp 157 - 155 °C (from $CHCl_3$). ^{1}H NMR (300 MHz, acetone-*d*6) δ 8.06 (br s, 1H), 7.61 (br s, 1H), 7.07 (br s, 1H), 6.97 (br d, *J* = 9.0 Hz, 1H), 6.87 (dt, *J* = 10.4 Hz, 1H), 4.03 (s, 3H); ^{19}F NMR (250 MHz, $CDCl_3$) δ −110.01;^{13}C NMR (90.5 MHz, acetone-*d*6) δ 192.4, 164.0 (d, *J* = 244.3 Hz), 159.7 (d, *J* = 11.6 Hz), 155.1, 142.1 (d, *J* = 9.2 Hz), 135.1, 125.5, 120.3, 113.1, 112.3, 107.6 (d, *J* = 23.2 Hz), 106.4 (d, *J* = 24.2 Hz), 57.2. HRMS (ESI-) calcd. for $[C_{14}H_{10}FNO_6\text{-H}]^-$ 306.0414; found $[M - H]^-$ 306.0424.

4.3. Recombinant TTR expression and purification

The cDNA encoding for WT-TTR was cloned into a pET28a vector (Novagen). The vectors encoding for V30M- and V122I-TTR were prepared by classical site-directed mutagenesis protocols using the WT-TTR vector as a template. WT-, V30M- and V122I-TTR were expressed in *Escherichia coli* BL21 (DE3) and purified as previously described [26]. The purest fractions eluting from the gel filtration chromatography were combined and kept at −20 °C until use. The concentration of protein was determined spectrophotometrically at 280 nm, using a molar extinction coefficient of 77 600 M^{-1} cm^{-1}.

4.4. Urea-induced TTR tetramer dissociation measured by Trp fluorescence

Samples containing TTR (1.8 μM in PBS) were incubated with 3.6 μM **PITB** or tolcapone for 30 min at RT, and 6 M urea was added to trigger denaturation. Since the stock solutions of both compounds were prepared in DMSO, a control sample containing the same percentage of DMSO instead of compound was prepared. Trp fluorescence spectra were recorded over time (λ_{ex} = 295 nm; λ_{em} = 310–410 nm) using an FP-8200 Spectrofluorometer (Jasco). Upon denaturation, the Trp residues become more exposed to the polar solvent, which is accompanied by a change in the emission maximum from ~335 to ~355 nm. The fluorescence intensity ratio 355/335 nm was calculated for each time point and the values normalized from minimum (folded state) to maximum (unfolded state), with the maximum being the one of the control sample after 96 h incubation.

4.5. TTR in vitro aggregation inhibition

To assess the effect of **PITB** and tolcapone in the aggregation of WT-, V30M- and V122I-TTR, a well-established TTR aggregation assay was employed [31,51]. Briefly, TTR solutions (7.2 μM in 10 mM sodium phosphate, 100 mM KCl, 1 mM EDTA, 1 mM DTT, pH 7.0) were incubated with varying concentrations of test compound for 30 min at 37 °C. The percentage of DMSO was the same in all samples (5%). Following incubation, the pH of the solutions was dropped to 4.2 via addition of an equal volume of acidification buffer (100 mM sodium acetate, 100 mM KCl, 1 mM EDTA, 1 mM DTT, pH 4.2) and the samples were kept at 37 °C for more 72 h. The aggregation was assessed by measuring turbidity at 340 nm using a Varian Cary Eclipse Fluorescence Spectrophotometer (Agilent Technologies). Since **PITB** and tolcapone display dose-dependent absorbance at 340 nm, the turbidity of a sample containing the same concentration of compound, but lacking TTR, was subtracted to every measurement. The percentage of TTR aggregation for each inhibitor concentration was calculated by dividing the turbidity of the test sample by that of a sample aggregated in the absence of compound, and multiply by 100.

4.6. Isothermal titration calorimetry

All ITC measurements were carried out with protein and compounds dissolved in the same buffer (in a PBS buffer pH 7.0 containing 100 mM KCl, 1 mM EDTA and 2.5% DMSO), and degassed. The ITC measurements were performed at 25 °C using a Nano ITC calorimeter (TA Instruments). Titrations were performed as a set of 20 injections of 100 μM compound into protein (5 μM), programmed as a 2.02 μl injection with 150 s of equilibration period. The NanoAnalyze software (TA Instruments) was used to integrate the peaks and evaluate heat effects per injection. The fittings were performed with a general model for a protein with two-ligand binding sites implemented in Origin 7.0 (OriginLab), which allows to establish if the binding is cooperative or non-cooperative [35,36].

4.7. Crystallization and structure determination

Cocrystals of WT-TTR/**PITB**, V30M-TTR/**PITB**, V122I-TTR/**PITB** and V30M-TTR/tolcapone were obtained following previously described methods [26]. In brief, purified proteins (140 μM) were mixed with 1.4 mM of **PITB**/tolcapone and co-crystallized at 18 °C using the hanging-drop vapor diffusion technique. The reservoir solution consisted of 20–30% PEG 400, 200 mM $CaCl_2$, and 100 mM HEPES, with a pH range of 7.0–8.0. The crystals were rapidly frozen in liquid nitrogen (100 K), and diffraction data were collected at the BL13-XALOC beamline from the ALBA Synchrotron in Barcelona [52]. Data integration and merging were performed using XDS [53], and further analysis was conducted with CCP4 [54], including scaling and reduction of the data. The structures of the TTR/**PITB** and V30M-TTR/tolcapone complexes were determined from the X-ray data through molecular replacement with Phenix (version 1.19.2–4158) [55], utilizing a previously solved TTR structure (PDB 1F41) as a reference model. Model refinement and building were carried out using Phenix [55] and Coot [56], respectively. Refinement and data statistics can be found in Table S1. The atomic coordinates have been deposited in the PDB [PDB accession codes 8PM9 (**PITB**:WT), 8PMA (**PITB**:V30M), 8PMO (**PITB**:V122I), and 8PM8 (Tolcapone:V30M)]. The structural representations were generated using Pymol (The PyMOL Molecular Graphics System, Version 2.0, Schrödinger, LLC).

4.8. T_4 binding competition assays

The ability of **PITB** and tolcapone to displace T_4 from plasmatic TTR was evaluated by incubation of whole plasma (5 μl) with 1 μl of [^{125}I]-T_4 (specific radioactivity 1250 μCi/μg; concentration 320 μCi/mL; PerkinElmer) in the presence of the test compounds (5 molar excess relative to TTR tetramer). A negative control containing the same percentage of DMSO than the samples was also prepared. Following 1 h incubation at room temperature, plasma proteins were separated by native PAGE [40], the gels were dried, and subjected to phosphor imaging using a Typhoon 8600 variable mode imager (Molecular Diagnostics, Amersham Biosciences). Then, the autoradiography films were scanned, and the bands quantified using Image Lab software version 5.2.1 (Bio-Rad). The amount of T_4 bound to TTR in comparison to total T_4 (T_4-TBG + T_4-ALB + T_4-TTR) was determined for each sample and normalized to the maximum value, which corresponds to the negative control. Plasma from three control individuals (WT-TTR) and three TTR V30M carriers was analyzed.

4.9. TTR stabilization in human plasma assessed by isoelectric focusing

To assess the effect of **PITB** and tolcapone on the stability of TTR in plasma, isoelectric focusing (IEF) under semi-denaturing conditions was

performed [41]. To carry out this assay, 30 μl of human plasma from control individuals (n = 2) or TTR V30M carriers (n = 3) were incubated overnight at 4 °C in the presence of 19.1 μM compounds. Additionally, control samples containing the same amount of DMSO rather than compound were prepared. After incubation, the samples were subjected to native PAGE, and the TTR gel band was excised and applied to an IEF gel. IEF was performed in the presence of 4 M urea (semi-denaturing conditions) and 5% (v/v) ampholytes (pH 4–6.5; Sigma-Merck), at 1200 V for 5 h. Proteins were then fixed with 20% trichloroacetic acid and stained with Coomassie blue. The gels were scanned using a GS-900 calibrated densitometer (Bio-Rad) and the bands analyzed by densitometry with the Image Lab software version 5.2.1 (Bio-Rad). The ratio of the TTR tetramer over total TTR (TTR tetramer + monomer) was determined for each sample, and the percentage of tetramer stabilization was calculated as ((ratio treated sample − ratio control sample)/ratio control sample) × 100.

4.10. Cytotoxicity studies

The potential chemical toxicity of **PITB** was evaluated in vitro in HeLa, HepG2 and MRC-5 human cell lines. Tolcapone was tested in parallel for comparison. HeLa, HepG2 and MRC-5 cells were cultured in MEM ALPHA medium (Gibco) supplemented with 10% fetal bovine serum at 37 °C in a 5% CO_2 humidified atmosphere. Cells were seeded in 96-well plates at 3500 cells/well (HeLa), 4500 cells/well (HepG2) or 1500 cells/well (MRC-5) and incubated with increasing concentrations of compound (2–100 μM) for 72 h at 37 °C. Controls were prepared with the equivalent amount of DMSO relative to each concentration of compound. Then, 10 μl of PrestoBlue® reagent (Thermo Fisher Scientific) were added to each well, and after incubating for 15 min at 37 °C, the fluorescence emission was recorded using either a 590/20 filter with an excitation wavelength of 535 nm in a Victor3 Multilabel Reader (PerkinElmer) or a monochromator (λ_{ex} = 560 nm; λ_{em} = 590 nm) in a Spark® multimode microplate reader (Tecan). The assays were performed in triplicate and the percentage of cell viability for each well was calculated as (intensity sample − mean intensity blank)/(mean intensity control – mean intensity blank) × 100, where ″mean intensity blank″ corresponds to the mean intensity of wells with PrestoBlue® alone and ″mean intensity control″ is the mean intensity of wells that contain the corresponding percentage of DMSO.

4.11. In vivo pharmacokinetic studies in mice

The PK studies of M-23 (IV and PO), **PITB** (IV and PO) and tolcapone (PO) in CD-1 mice were conducted by Draconis Pharma S.L. For each study, 24 male CD-1 mice were weighted and identified by a distinct number at the base of the tail. The animals were maintained in accordance with: European Directive for the Protection of Vertebrate Animals Used for Experimental and other Scientific Purposes (86/609/EU), Decree 214/1997 of 30th July. Ministry of agriculture, livestock and fishing of the Autonomous Government of Catalonia, Spain, and Royal Decree 53/2013 of 1st February (Spain). All the experimental procedures were approved by the Animal Experimentation Ethical Committee of the Autonomous University of Barcelona and by the Animal Experimentation Commission of the Autonomous Government of Catalonia. DAAM:9678.

For the IV studies, M-23 was dissolved in PBS and **PITB** in 5% Cremophor/5% Mannitol/5% DMSO. Both compounds were administered at 1 mg/kg, with an administration volume of 5 mL/kg. At different timepoints after administration (0.0833, 0.5, 1, 2, 4, 6 and 24 h), three animals were anesthetized with isoflurane, and their blood collected by cava vein puncture in tubes containing K2-EDTA 5%. Three animals were not administered and referred as t = 0 h (predose). Blood samples were centrifuged at 10 000 rpm for 5 min to obtain the plasmas, which were stored at −80 °C until analysis. For the PO studies, M-23, **PITB** and tolcapone were formulated in 0.5% CMC/0.1% tween 80 and administered at 10 mg/kg. The administered volume was 10 mL/kg. Plasma samples were obtained as described above at 0.25, 0.5, 1, 2, 4, 6 and 24 h post-dosing (three animals for time point). Three animals were used as blank with no administration (predose). All plasma samples were analyzed using the API 3200 LC-MS/MS system (Sciex) coupled to an UPLC-Acquity (Waters). A calibration curve was done for each compound in plasma. The lower limit of quantification (LLOQ) for M-23, **PITB** and tolcapone were 2.93 ng/mL, 7.68 ng/mL and 2.73 ng/mL, respectively. For **PITB** quantification in plasma samples from the PK studies of M-23 (IV and PO), the same UPLC-MS/MS detection system was used. The calibration curve done for **PITB** PK studies was applied in this case. PK parameters were determined with a non-compartmental model using Phoenix 64 8.3 (WinNolin) software.

Declaration of competing interest

Authors have submitted a patent application on the basis of the here presented research. It is protected the use of **PITB** as a therapy for TTR amyloidosis. Inventors: S.V., I.P, F.P., D.R., N.V., R.A., F.B., A.S Title: Compound for the treatment of transthyretin amyloidosis. Property: Universitat Autònoma de Barcelona. Request number: EP2023/025333. All other authors declare no competing interests.

Data availability

Data will be made available on request.

Acknowledgements

This work was funded by the Spanish Ministry of Science and Innovation (PDC2021-120914-I00 to S.V. and PID2021-124602OB-I00 to D. R), and by the Universitat Autònoma de Barcelona (PROOF OF CONCEPT 2020) and ICREA, ICREA-Academia 2015 and 2020 to S.V. R. A. acknowledges the financial support of the Spanish Ministry of Economy and Competitiveness (PID2019-106403RB-I00). A.V.C acknowledges the Spanish Ministry of Science and Innovation MCIN/AEI/10.13039/501100011033/and "ERDF A way of Making Europe" (PID2021-127296OB-I00). F.P. and A.S. acknowledge the Universitat Autònoma de Barcelona for their doctoral grant. This work was funded by FCT—Fundação para a Ciência e a Tecnologia, I.P., under the project UIDB/04293/2020 to M.R.A., and through the support of F.B. with a PhD fellowship (SFRH/BD/123674/2016).

Appendix A. Supplementary data

Supplementary data to this article can be found online at https://doi.org/10.1016/j.ejmech.2023.115837.

References

[1] F. Chiti, C.M. Dobson, Protein misfolding, functional amyloid, and human disease, Annu. Rev. Biochem. 75 (2006) 333–366.
[2] H. Koike, M. Katsuno, Transthyretin amyloidosis: update on the clinical spectrum, pathogenesis, and disease-modifying therapies, Neurol Ther 9 (2020) 317–333.
[3] G.A. Hagen, W.J. Elliott, Transport of thyroid hormones in serum and cerebrospinal fluid, J. Clin. Endocrinol. Metab. 37 (1973) 415–422.
[4] G. Schreiber, A.R. Aldred, A. Jaworowski, C. Nilsson, M.G. Achen, M.B. Segal, Thyroxine transport from blood to brain via transthyretin synthesis in choroid plexus, Am. J. Physiol. 258 (1990) R338–R345.
[5] J. Magalhaes, J. Eira, M.A. Liz, The role of transthyretin in cell biology: impact on human pathophysiology, Cell. Mol. Life Sci. 78 (2021) 6105–6117.
[6] A. Carroll, P.J. Dyck, M. de Carvalho, M. Kennerson, M.M. Reilly, M.C. Kiernan, S. Vucic, Novel approaches to diagnosis and management of hereditary transthyretin amyloidosis, J. Neurol. Neurosurg. Psychiatry 93 (2022) 668–678.
[7] D.M. Rowczenio, I. Noor, J.D. Gillmore, H.J. Lachmann, C. Whelan, P.N. Hawkins, L. Obici, P. Westermark, G. Grateau, A.D. Wechalekar, Online registry for mutations in hereditary amyloidosis including nomenclature recommendations, Hum. Mutat. 35 (2014) E2403–E2412.
[8] C. Andrade, A peculiar form of peripheral neuropathy; familiar atypical generalized amyloidosis with special involvement of the peripheral nerves, Brain 75 (1952) 408–427.

[9] F.L. Ruberg, M. Grogan, M. Hanna, J.W. Kelly, M.S. Maurer, Transthyretin amyloid cardiomyopathy: JACC state-of-the-art review, J. Am. Coll. Cardiol. 73 (2019) 2872–2891.
[10] H. Goren, M.C. Steinberg, G.H. Farboody, Familial oculoleptomeningeal amyloidosis, Brain 103 (1980) 473–495.
[11] P. Westermark, K. Sletten, B. Johansson, G.G. Cornwell 3rd, Fibril in senile systemic amyloidosis is derived from normal transthyretin, Proc. Natl. Acad. Sci. U. S.A. 87 (1990) 2843–2845.
[12] M. Tanskanen, T. Peuralinna, T. Polvikoski, I.L. Notkola, R. Sulkava, J. Hardy, A. Singleton, S. Kiuru-Enari, A. Paetau, P.J. Tienari, L. Myllykangas, Senile systemic amyloidosis affects 25% of the very aged and associates with genetic variation in alpha2-macroglobulin and tau: a population-based autopsy study, Ann. Med. 40 (2008) 232–239.
[13] G.G. Cornwell 3rd, W.L. Murdoch, R.A. Kyle, P. Westermark, P. Pitkanen, Frequency and distribution of senile cardiovascular amyloid. A clinicopathologic correlation, Am. J. Med. 75 (1983) 618–623.
[14] P. Hammarstrom, X. Jiang, A.R. Hurshman, E.T. Powers, J.W. Kelly, Sequence-dependent denaturation energetics: a major determinant in amyloid disease diversity, Proc. Natl. Acad. Sci. U.S.A. 99 (Suppl 4) (2002) 16427–16432.
[15] A.R. Hurshman Babbes, E.T. Powers, J.W. Kelly, Quantification of the thermodynamically linked quaternary and tertiary structural stabilities of transthyretin and its disease-associated variants: the relationship between stability and amyloidosis, Biochemistry 47 (2008) 6969–6984.
[16] P. Hammarstrom, R.L. Wiseman, E.T. Powers, J.W. Kelly, Prevention of transthyretin amyloid disease by changing protein misfolding energetics, Science 299 (2003) 713–716.
[17] S.M. Johnson, R.L. Wiseman, Y. Sekijima, N.S. Green, S.L. Adamski-Werner, J. W. Kelly, Native state kinetic stabilization as a strategy to ameliorate protein misfolding diseases: a focus on the transthyretin amyloidoses, Acc. Chem. Res. 38 (2005) 911–921.
[18] C.E. Bulawa, S. Connelly, M. Devit, L. Wang, C. Weigel, J.A. Fleming, J. Packman, E.T. Powers, R.L. Wiseman, T.R. Foss, I.A. Wilson, J.W. Kelly, R. Labaudiniere, Tafamidis, a potent and selective transthyretin kinetic stabilizer that inhibits the amyloid cascade, Proc. Natl. Acad. Sci. U.S.A. 109 (2012) 9629–9634.
[19] F.A. Barroso, D.P. Judge, B. Ebede, H. Li, M. Stewart, L. Amass, M.B. Sultan, Long-term safety and efficacy of tafamidis for the treatment of hereditary transthyretin amyloid polyneuropathy: results up to 6 years, Amyloid 24 (2017) 194–204.
[20] M.S. Maurer, J.H. Schwartz, B. Gundapaneni, P.M. Elliott, G. Merlini, M. Waddington-Cruz, A.V. Kristen, M. Grogan, R. Witteles, T. Damy, B. M. Drachman, S.J. Shah, M. Hanna, D.P. Judge, A.I. Barsdorf, P. Huber, T. A. Patterson, S. Riley, J. Schumacher, M. Stewart, M.B. Sultan, C. Rapezzi, A.-A. S. Investigators, Tafamidis treatment for patients with transthyretin amyloid cardiomyopathy, N. Engl. J. Med. 379 (2018) 1007–1016.
[21] C. Monteiro, J.S. Mesgazardeh, J. Anselmo, J. Fernandes, M. Novais, C. Rodrigues, G.J. Brighty, D.L. Powers, E.T. Powers, T. Coelho, J.W. Kelly, Predictive model of response to tafamidis in hereditary ATTR polyneuropathy, JCI Insight (2019) 4.
[22] D.S. Kazi, B.K. Bellows, S.J. Baron, C. Shen, D.J. Cohen, J.A. Spertus, R.W. Yeh, S. V. Arnold, B.W. Sperry, M.S. Maurer, S.J. Shah, Cost-effectiveness of tafamidis therapy for transthyretin amyloid cardiomyopathy, Circulation 141 (2020) 1214–1224.
[23] R. Sant'Anna, P. Gallego, L.Z. Robinson, A. Pereira-Henriques, N. Ferreira, F. Pinheiro, S. Esperante, I. Pallares, O. Huertas, M.R. Almeida, N. Reixach, R. Insa, A. Velazquez-Campoy, D. Reverter, N. Reig, S. Ventura, Repositioning tolcapone as a potent inhibitor of transthyretin amyloidogenesis and associated cellular toxicity, Nat. Commun. 7 (2016), 10787.
[24] N. Reig, S. Ventura, M. Salvadó, J. Gámez, R. Insa, SOM0226, a repositioned compound for the treatment of TTR amyloidosis, Orphanet J. Rare Dis. 10 (2015) P9.
[25] J. Gamez, M. Salvado, N. Reig, P. Sune, C. Casasnovas, R. Rojas-Garcia, R. Insa, Transthyretin stabilization activity of the catechol-O-methyltransferase inhibitor tolcapone (SOM0226) in hereditary ATTR amyloidosis patients and asymptomatic carriers: proof-of-concept study(and), Amyloid 26 (2019) 74–84.
[26] F. Pinheiro, N. Varejao, S. Esperante, J. Santos, A. Velazquez-Campoy, D. Reverter, I. Pallares, S. Ventura, Tolcapone, a potent aggregation inhibitor for the treatment of familial leptomeningeal amyloidosis, FEBS J. 288 (2021) 310–324.
[27] F. Pinheiro, I. Pallares, F. Peccati, A. Sanchez-Morales, N. Varejao, F. Bezerra, D. Ortega-Alarcon, D. Gonzalez, M. Osorio, S. Navarro, A. Velazquez-Campoy, M. R. Almeida, D. Reverter, F. Busque, R. Alibes, M. Sodupe, S. Ventura, Development of a highly potent transthyretin amyloidogenesis inhibitor: design, synthesis, and evaluation, J. Med. Chem. 65 (2022) 14673–14691.
[28] K. Jorga, B. Fotteler, P. Heizmann, R. Gasser, Metabolism and excretion of tolcapone, a novel inhibitor of catechol-O-methyltransferase, Br. J. Clin. Pharmacol. 48 (1999) 513–520.
[29] V. Loconte, M. Cianci, I. Menozzi, D. Sbravati, F. Sansone, A. Casnati, R. Berni, Interactions of tolcapone analogues as stabilizers of the amyloidogenic protein transthyretin, Bioorg. Chem. 103 (2020), 104144.
[30] P. Hammarstrom, X. Jiang, S. Deechongkit, J.W. Kelly, Anion shielding of electrostatic repulsions in transthyretin modulates stability and amyloidosis: insight into the chaotrope unfolding dichotomy, Biochemistry 40 (2001) 11453–11459.
[31] X. Jiang, J.N. Buxbaum, J.W. Kelly, The V122I cardiomyopathy variant of transthyretin increases the velocity of rate-limiting tetramer dissociation, resulting in accelerated amyloidosis, Proc. Natl. Acad. Sci. U.S.A. 98 (2001) 14943–14948.
[32] L. Saelices, L.M. Johnson, W.Y. Liang, M.R. Sawaya, D. Cascio, P. Ruchala, J. Whitelegge, L. Jiang, R. Riek, D.S. Eisenberg, Uncovering the mechanism of aggregation of human transthyretin, J. Biol. Chem. 290 (2015) 28932–28943.
[33] S.C. Penchala, S. Connelly, Y. Wang, M.S. Park, L. Zhao, A. Baranczak, I. Rappley, H. Vogel, M. Liedtke, R.M. Witteles, E.T. Powers, N. Reixach, W.K. Chan, I. A. Wilson, J.W. Kelly, I.A. Graef, M.M. Alhamadsheh, AG10 inhibits amyloidogenesis and cellular toxicity of the familial amyloid cardiomyopathy-associated V122I transthyretin, Proc. Natl. Acad. Sci. U.S.A. 110 (2013) 9992–9997.
[34] R.N. Ferguson, H. Edelhoch, H.A. Saroff, J. Robbins, H.J. Cahnmann, Negative cooperativity in the binding of thyroxine to human serum prealbumin. Preparation of tritium-labeled 8-anilino-1-naphthalenesulfonic acid, Biochemistry 14 (1975) 282–289.
[35] S. Vega, O. Abian, A. Velazquez-Campoy, A unified framework based on the binding polynomial for characterizing biological systems by isothermal titration calorimetry, Methods 76 (2015) 99–115.
[36] E. Freire, A. Schon, A. Velazquez-Campoy, Isothermal titration calorimetry: general formalism using binding polynomials, Methods Enzymol. 455 (2009) 127–155.
[37] Y.T. Liu, Y.J. Yen, F. Ricardo, Y. Chang, P.H. Wu, S.J. Huang, K.P. Lin, T.Y. Yu, Biophysical characterization and modulation of transthyretin Ala97Ser, Ann Clin Transl Neurol 6 (2019) 1961–1970.
[38] E. Morais-de-Sa, P.J. Pereira, M.J. Saraiva, A.M. Damas, The crystal structure of transthyretin in complex with diethylstilbestrol: a promising template for the design of amyloid inhibitors, J. Biol. Chem. 279 (2004) 53483–53490.
[39] M.P. Sebastiao, V. Lamzin, M.J. Saraiva, A.M. Damas, Transthyretin stability as a key factor in amyloidogenesis: X-ray analysis at atomic resolution, J. Mol. Biol. 306 (2001) 733–744.
[40] M.R. Almeida, B. Macedo, I. Cardoso, I. Alves, G. Valencia, G. Arsequell, A. Planas, M.J. Saraiva, Selective binding to transthyretin and tetramer stabilization in serum from patients with familial amyloidotic polyneuropathy by an iodinated diflunisal derivative, Biochem. J. 381 (2004) 351–356.
[41] N. Ferreira, I. Cardoso, M.R. Domingues, R. Vitorino, M. Bastos, G. Bai, M. J. Saraiva, M.R. Almeida, Binding of epigallocatechin-3-gallate to transthyretin modulates its amyloidogenicity, FEBS Lett. 583 (2009) 3569–3576.
[42] W.G. Schoonen, W.M. Westerink, J.A. de Roos, E. Debiton, Cytotoxic effects of 100 reference compounds on Hep G2 and HeLa cells and of 60 compounds on ECC-1 and CHO cells. I mechanistic assays on ROS, glutathione depletion and calcein uptake, Toxicol. Vitro 19 (2005) 505–516.
[43] M.I. Thabrew, R.D. Hughes, I.G. McFarlane, Screening of hepatoprotective plant components using a HepG2 cell cytotoxicity assay, J. Pharm. Pharmacol. 49 (1997) 1132–1135.
[44] B. Ekwall, Toxicity to HeLa cell of 205 drugs as determined by the metabolic inhibition test supplemented by microscopy, Toxicology 17 (1980) 273–295.
[45] Z. Mostafavi-Pour, F. Khademi, F. Zal, A.R. Sardarian, F. Amini, In vitro analysis of CsA-induced hepatotoxicity in HepG2 cell line: oxidative stress and alpha2 and beta1 integrin subunits expression, Hepat. Mon. 13 (2013), e11447.
[46] R. Krithika, R.J. Verma, P.S. Shrivastav, Antioxidative and cytoprotective effects of andrographolide against CCl4-induced hepatotoxicity in HepG2 cells, Hum. Exp. Toxicol. 32 (2013) 530–543.
[47] W.M. Lee, Drug-induced hepatotoxicity, N. Engl. J. Med. 349 (2003) 474–485.
[48] C.W. Olanow, Tolcapone and hepatotoxic effects. Tasmar advisory panel, Arch. Neurol. 57 (2000) 263–267.
[49] R.M. Weinshilboum, D.M. Otterness, C.L. Szumlanski, Methylation pharmacogenetics: catechol O-methyltransferase, thiopurine methyltransferase, and histamine N-methyltransferase, Annu. Rev. Pharmacol. Toxicol. 39 (1999) 19–52.
[50] S. Rendic, Summary of information on human CYP enzymes: human P450 metabolism data, Drug Metab. Rev. 34 (2002) 83–448.
[51] X. Jiang, C.S. Smith, H.M. Petrassi, P. Hammarstrom, J.T. White, J.C. Sacchettini, J.W. Kelly, An engineered transthyretin monomer that is nonamyloidogenic, unless it is partially denatured, Biochemistry 40 (2001) 11442–11452.
[52] J. Juanhuix, F. Gil-Ortiz, G. Cuni, C. Colldelram, J. Nicolas, J. Lidon, E. Boter, C. Ruget, S. Ferrer, J. Benach, Developments in optics and performance at BL13-XALOC, the macromolecular crystallography beamline at the ALBA synchrotron, J. Synchrotron Radiat. 21 (2014) 679–689.
[53] W. Kabsch, Integration, scaling, space-group assignment and post-refinement, Acta Crystallogr D Biol Crystallogr 66 (2010) 133–144.
[54] M.D. Winn, C.C. Ballard, K.D. Cowtan, E.J. Dodson, P. Emsley, P.R. Evans, R. M. Keegan, E.B. Krissinel, A.G. Leslie, A. McCoy, S.J. McNicholas, G.N. Murshudov, N.S. Pannu, E.A. Potterton, H.R. Powell, R.J. Read, A. Vagin, K.S. Wilson, Overview of the CCP4 suite and current developments, Acta Crystallogr D Biol Crystallogr 67 (2011) 235–242.
[55] P.D. Adams, P.V. Afonine, G. Bunkoczi, V.B. Chen, I.W. Davis, N. Echols, J. J. Headd, L.W. Hung, G.J. Kapral, R.W. Grosse-Kunstleve, A.J. McCoy, N. W. Moriarty, R. Oeffner, R.J. Read, D.C. Richardson, J.S. Richardson, T. C. Terwilliger, P.H. Zwart, PHENIX: a comprehensive Python-based system for macromolecular structure solution, Acta Crystallogr D Biol Crystallogr 66 (2010) 213–221.
[56] P. Emsley, B. Lohkamp, W.G. Scott, K. Cowtan, Features and development of Coot, Acta Crystallogr D Biol Crystallogr 66 (2010) 486–501.